International Journal of Automotive Technology, Vol. 6, No. 3, pp. 277–283 (2005)

1229-9138/2005/021-11

AUTOMOTIVE FORMABILITY SIMULATION PROCESS FOR EARLY DESIGN PHASES

J. EL-SAYED[1)*], H. KIM[1)], R. FRUTIGER[2)] and W. LIU[2)]

[1)]Kettering University, Flint, MI 48504, USA.
[2)]General Motors, Warren, MI 48090, USA.

(Received 15 June 2004; Revised 22 October 2004)

ABSTRACT–Formability simulation of automotive panels at early design phases can reduce product and tooling development time and cost. However, for the simulation to be effective in leading the design process, fast and reliable results should be achieved with limited design definition and minimum modeling effort. In this paper, nonlinear finite element analysis is used to develop an automated process for the formability simulation of automotive body panels at early design phases. Due to the limited design definition at early design phases, the automated simulation process is based on the plane strain analysis for selected number of typical sections along the panel. Therefore, an entire panel can be analyzed with few sections. The state of plane strain can be easily induced, during simulation through symmetry and applied boundary conditions that simplify the modeling process. To study the reliability and effectiveness of the developed simulation process, the analytical results are compared with measured results of production automotive body side panels. The comparison demonstrates that the developed simulation process is reliable and can be effective for analyzing sheet metal formability, in early vehicle development phases.

KEY WORDS : Plane strain, Formability, Simulation process, Automotive panels, Early design phases

1. INTRODUCTION

For mass production of sheet metal parts with complicated geometry such as inner and outer panels sheet metal forming is the most common manufacturing process. A sheet metal forming process usually has several input variables. These variables relate the sheet blank (geometry and material), the tools (geometry and material), the conditions at the tool-material interface, the mechanics of plastic deformation, the equipment used, the characteristics of the final product, and finally the plant environment in which the process is being conducted. Some of the pioneering work on design of automotive panels and practical die design using section analysis are given in references (Keum and Wang, 1990; Soran *et al.*, 1991; Keum *et al.*, 1992).

To analyze the sheet metal forming process for potential forming defects such as splitting, wrinkling, and spring-back Finite Element Analysis (FEA) has become the main simulation tool (American Iron and Steel Institute, 1984; Hosford and Caddell, 1993; Kobayashi *et al.*, 1989; Wang *et al.*, 1999). Deep drawing simulation can be categorized as typical nonlinear finite element analysis characterized by geometric and material non-linearity. Preparing a detailed finite Element model for nonlinear analysis, however, is a very time consuming task. In addition, the geometric details of most automotive components are not usually very well defined at early design phases.

In order to speed up the automotive product design, development and manufacturing process tooling commitment needs to be made at early design phases. The objective of this paper is to present a fast and reliable approach for the formability simulation of automotive sheet metal sections to guide both product design and tooling specification at early design phases. To perform the formability simulation with limited number of cross sections defined, the plane strain approach can be used. The applicability of the plain strain approach is based on the fact that for a certain section location of a stamped panel, the minor strains are relatively negligible compared to the major strains and an entire panel can be analyzed with few sections. In this study, to automate the formability simulation process for the plane strain approach decoupled, implicit finite element software was used (Autoform, 1999).

To demonstrate the effectiveness and the reliability of the developed process, the analytical results of three

*Corresponding author. e-mail: jelsayed@kettering.edu

automotive sections are compared with measured data. The three side panel sections were simulated at the Rocker, A-Pillar, and B-pillar areas to cover a wide range of automotive sections.

2. FORAMABILITY SIMULATION PROCESS

To speed up component release and tooling commitment at early design phases a formability simulation process is needed in addition to all other necessary performance simulation processes. In the following, the steps for the developed formability simulation process are discussed.

2.1. Identify a Selected Number of Critical Sections

In order to simulate the drawing process with limited design definition fewer sections are needed along the automotive panel. These typical sections are usually defined at early phases based on design best practices. At each defined typical section the plane strain condition can be assumed and only a narrow strip need to be modeled for the finite element simulation. The symmetry condition can be used on both sides to maintain the minor strain equal or nearly equal to zero. The restraining forces can be applied to both cross-sectional directions, in opposite direction to the metal flow, to simulate the restraining forces due to the draw bead and the friction effects. For correlation with measurements, the same boundary conditions should be applied to the analytical model.

2.2. Develop Analytical Models for Selected Sections

In a forming process, binder force is applied to hold the sheet and restrain it from free flow. As a result of the restraining force, the final sheet can have desirable strain to maintain the final shape and have enough stiffness. However, to control the metal flow by only the binder force is not sufficient due to the limitation on the binder force capacity. In order to add more restraining force, draw bead can be used to control the metal flow (Cao and Boyce, 1993). The added metal flow control is achieved from the restraining force induced by the consecutive bending and unbending process along the draw bead geometry. This draw bead effect can be defined by adding draw bead geometry at the right position on the binder, or by applying a force on the draw bead line with a specific draw bead force factor.

The main purpose for using draw beads in the actual sheet metal forming process is to control the metal flow. For simulation, accurate modeling of the draw beads by including the effect of variable cross-sections, end effects, and work hardening within the material can improve the results. However, geometric draw bead modeling can increase the pre-processing time and computational costs. An alternative is to apply restraining forces along the centerlines of the draw bead geometry. This approach is evaluated in this work for its potential to reduce computer time and modeling efforts.

2.3. Determine Geometric and Material Properties

Due to variation in sheet metal thickness and material properties, provided by suppliers within a material specification, there is a need to identify the proper values to achieve good level of correlation. In this work, the initial sheet thickness was measured at arbitrary locations on the sheet. The readings ranged from 0.78 to 0.80 mm. The nominal value of 0.80 mm was used for the analytical simulation and the average value of 0.79 mm was used to calculate the percent thinning. It is also assumed that the material properties of the sheet in the stamping process and those of the computer simulation model are the same. Followings are the material properties for the SAE 1008 hot-rolled steel used:

Yield Strength (S_y)	174 MPa
Young's Modulus (E)	207 GPa
Poisson's ratio (n)	0.3
Yield Strain (e_y)	6.153 E-03
Strain-hardening Exponent (n)	0.221
Strength Coefficient (K)	536 MPa
Width-to-thickness strain ratio (R)	1.92

2.4. Select Proper Analysis Tools and Procedures

In a forming analysis, the tools such as die, punch, and binder are considered as rigid bodies, only the sheet blank has to deform to a final shape. Figures 1, 2 show the finite element models used in the plane strain simulation of the Rocker section, with and without draw beads respectively.

Tables 1, 2 contain the boundary conditions used in the analytical models for the Rocker, A-pillar and B-pillar section used in the study for the conditions with and without draw beads.

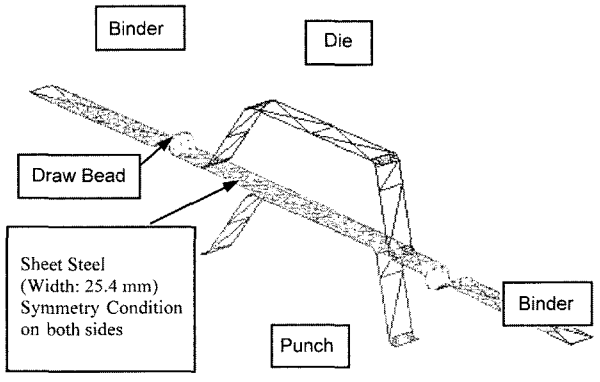

Figure 1. Model for Rocker section with draw bead.

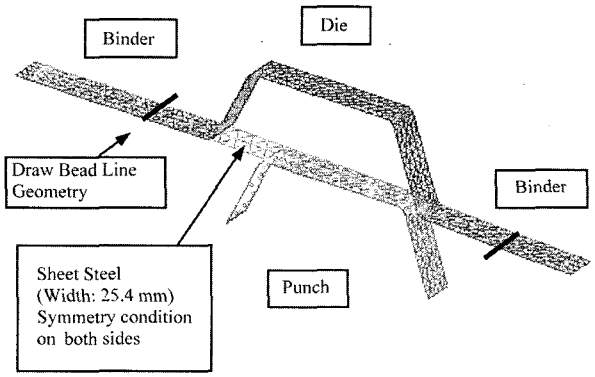

Figure 2. Model for Rocker section without draw bead.

Table 1. Boundary condition-models with draw beads.

	Section 1 (Rocker)		Section 2 (A-pillar)		Section 3 (B-pillar)	
D. Bead Location	Top	Bottom	Top	Bottom	Front	Rear
Force (N)	9300	4400	6800	6400	1900	300

Symmetry Condition: both sides
Sheet metal thickness: 0.80 mm
Friction Coefficient: 0.15 (default)

Table 2. Boundary condition-models without draw beads.

	Section 1 (Rocker)		Section 2 (A-pillar)		Section 3 (B-pillar)	
D. Bead Location	Top	Bottom	Top	Bottom	Front	Rear
DB Force Factor	1.15	1.05	0.95	1.02	1.00	0.93

Symmetry Condition: both sides
Sheet metal thickness: 0.80 mm
Friction Coefficient: 0.15 (default)
Binder Pressure: 200 N/mm^2

3. CORRELATION WITH MEASUREMENTS

To correlate the analytical results with measurements, an early production phase automotive body side panel was used. Three sections along the Rocker, A-Pillar, and B-Pillar on the body side panel were marked, as shown in Figure 3. These locations were selected as the critical sections for formability and other vehicle performance aspects such as stiffness, dynamic behavior, and durability and crash worthiness. Correlation points along the selected sections were chosen based on the highest strain locations.

3.1. Measurements

For the selected sections, the draw-in amount and % thinning were used to correlate between the measured and analytical results. To determine the draw-in amount length measurements were conducted before and after forming. The length measurements were performed on the initial and final drawn panel using a plastic tape and strip ruler. The plastic tape was attached to the panel and marked at each draw bead radii to measure the distance between the draw beads and the distance from each draw bead radius to the end of the panel when detached from the panel. Initial length of the virign blank sheet was measured using a strip ruler. The measurement results were then used in the length of line analysis to calculate the draw-in amounts. Usually small error can be introduced with this measuring procedure. Also, there might be some deviations on the point locations between measurement and simulation. Some of these differences between the simulation model (CAD) data and the actual panel are shown in Table 3.

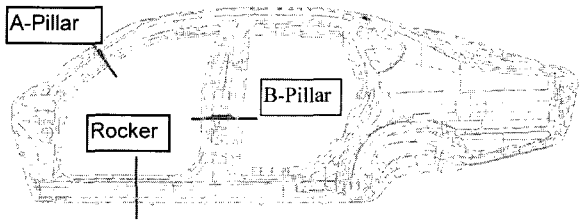

Figure 3. Section locations on the automotive panel.

To calculate the % thinning along the sections, thickness measurements were conducted before and after forming. Measurement points along the sections are selected based on highest strain location. Because of the limitations on the application of the thickness gauge, which has 5 mm diameter of probe and has to be firmly pressed to the panel, flat surface areas were chosen for measurements. The thickness measurement results were then converted to the percent thinning distributions presented in the following section.

3.2. Correlation Results

Using the analytical and measured results, the draw-in amounts were compared. The comparison results are shown in Table 4, for all three sections and the two analytical simulation conditions with and without draw beads.

Table 4, show good correlations for all three sections within the level of accuracy in both measurements and analysis. It is also clear that for draw-in amounts the two draw beads modeling conditions yield close results.

Figure 4, shows the comparison between the measured and analytical results in the % thinning at different points along the Rocker section. The analytical results are presented for both modeling conditions with and without draw beads. From the figure it is clear that the % thinning

Table 3. Arc radii of CAD data and measurement.

	Section 2 (A-pillar)		Section 3 (B-pillar)	
	Measurement	CAD data	Measurement	CAD data
Arc 1	5.8	7	6.8	5.8
Arc 2	20	20	3	2.5
Arc 3	11.3	13	5.3	3.2
Arc 4	10.5	11.5	6	5.9
Arc 5	4.5	4.8	6	5.8
Arc 6	6.8	6.5	6.8	6.5
Arc 7	6	6.6	3	2.7
Arc 8	5.8	5.9	6.3	6.5
Arc 9	20	20		
Arc 10	20.8	26.5		

Table 4. Draw-in condition, models with draw beads.

	Section 1 (Rocker)		Section 2 (A-pillar)		Section 3 (B-pillar)	
Measured	15.0	42.0	38.0	40.0	42.0	43.0
Simulation With D. B.	15.05	42.64	39.04	40.19	41.89	42.47
Simulation Without D. B.	15.32	41.92	37.25	40.07	42.10	42.44

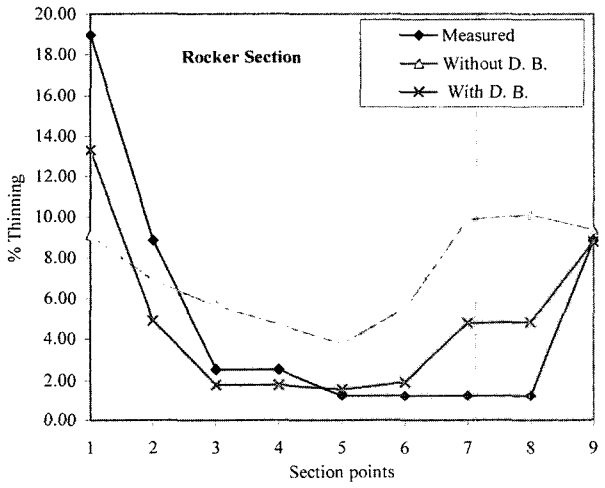

Figure 4. Rocker Section - % thinning distribution.

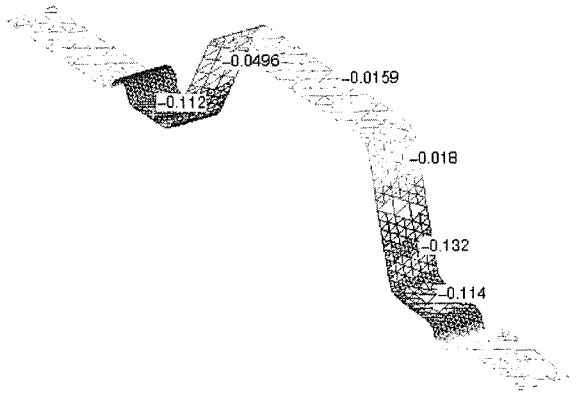

Figure 5. Rocker sec. %thinning contour, with D. B.

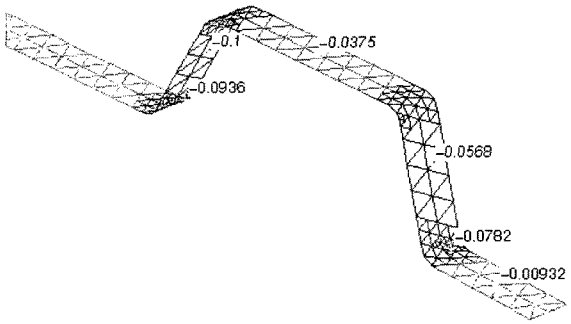

Figure 6. Rocker sec. %thinning contour, without D. B.

distribution for the model with draw beads is closer to the measured results than that of the model without the draw bead. In addition, the measurement and the model with draw beads show that the higher strains (% thinning) are near the draw beads, whereas in the analyses without draw bead geometry the higher strains are around the corners of the wall.

Figures 5, 6 show the analytical % thinning contours of the Rocker section for the models with draw beads and

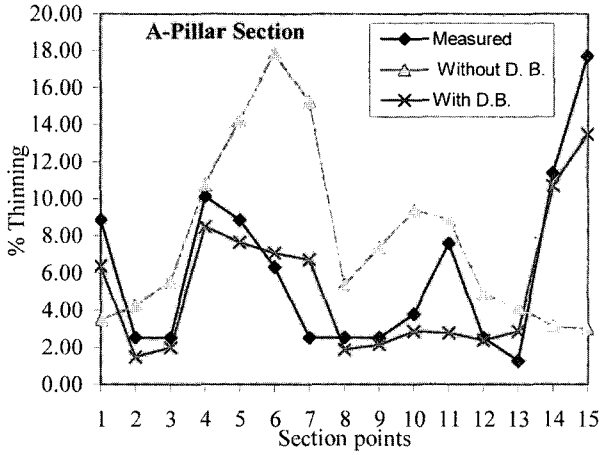

Figure 7. A-pillar Section – % thinning distribution.

without draw beads respectively. By comparing the two analytical contours, it is clear that the distributions along the sections are different.

Figure 7, shows the comparison between the measured and analytical results in the % thinning at different points along the A-pillar section.

The analytical results are presented for both modeling conditions with and without draw beads. Like the Rocker

Figure 8. A-pillar sec. %thinning contour, with D. B.

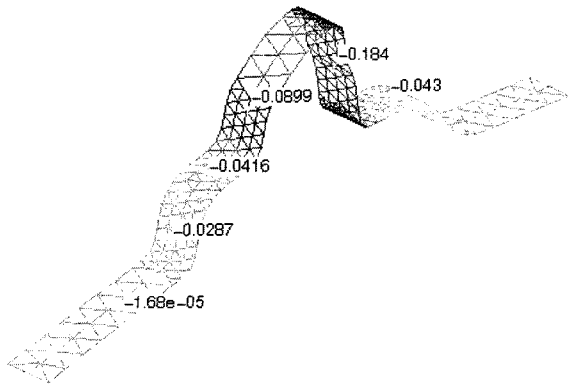

Figure 9. A-pillar sec. %thinning contour, without D. B.

section, from the figure it is clear that the % thinning distribution for the model with draw beads is closer to the measured results than that of the model without the draw bead. Also, the measurement and the model with draw beads show that the higher strains (% thinning) are near the draw beads, whereas in the analyses without draw bead geometry they are around the corners of the wall.

Figures 8, 9 show the analytical % thinning contours of the A-pillar section for the models with draw beads and without draw beads. It is clear that the stress distributions along the sections are different.

Figure 10 shows the comparison between the measured and analytical results in the % thinning at different points along the B-pillar section. The analytical results are presented for both modeling conditions with and without draw beads. From the figure it is clear that the % thinning distribution is close to the measured results for both models. In addition, the higher strains (% thinning) are around the corners of the wall for the measurement and the two models.

Figures 11, 12 show the analytical % thinning contours of the B-pillar section for the models with draw beads and without draw beads. It is clear that the stress distributions along the sections are different but closer than those of the Rocker and A-pillar sections.

In general, it can be noticed that there are some difference between the analytical and measured results in the strain (% thinning) distribution along the three sections. For deep and complicated sections, as in the case of the Rocker and A-pillar, the measurement and the model with draw bead showed that the higher strains are near the draw beads. This effect was not captured in the

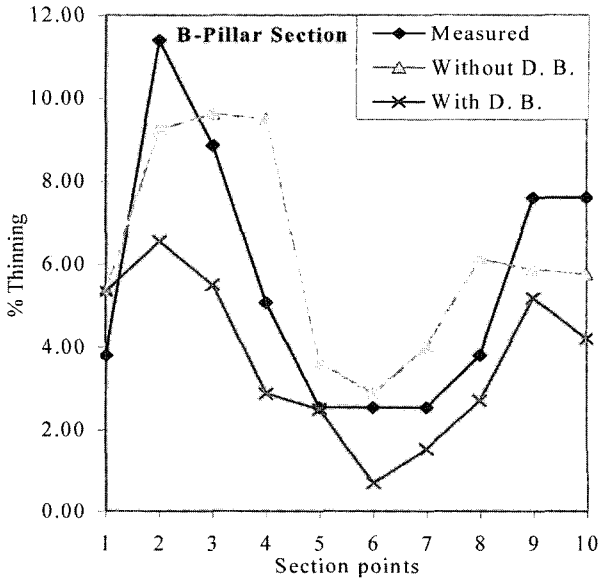

Figure 10. B-Pillar Section - % thinning distribution.

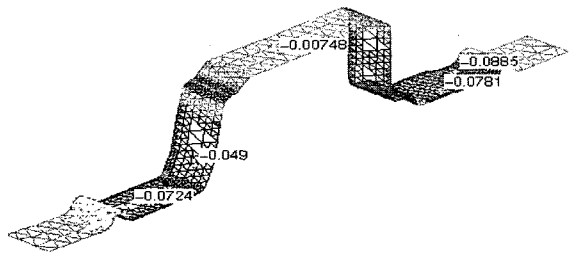

Figure 11. B-pillar sec. %thinning contour, with D. B.

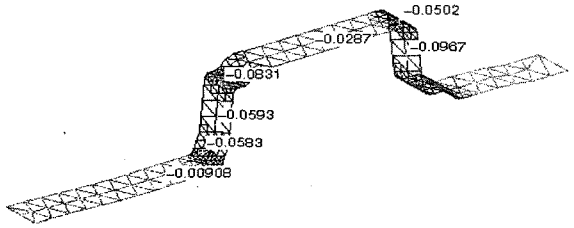

Figure 12. B-pillar sec. %thinning contour, without D. B.

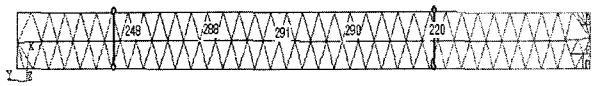

Figure 13. Stress distribution without draw bead geometry after closing step for the Rocker section.

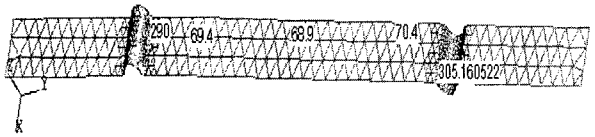

Figure 14. Stress distribution with draw bead geometry after closing step for the Rocker section.

model without the draw beads, and was not present in the shallow less complicated B-pillar section. The difference in the high strains distribution can be explained by investigating the plastic stress distribution after the closing step of the two analytical models. Figures 13, 14 show the stress distributions along the Rocker section for the models with the draw beads and without the draw beads. The stress level of the model without draw beads shows the highest stresses are distributed in the middle of the section, whereas the model with draw beads shows high stresses after the draw beads. In the case of draw bead geometry, the stress inside the draw beads are already in the plastic deformation region, and it is obvious that the metal in the plastic region can flow easier with the punch force than the metal in the elastic region. Because of these stress distributions, the models with draw bead geometry have better predictions than the models without draw bead geometry.

4. CONCLUSION

The main objective of this work is to develop an effective formability simulation process for analysis of automotive panels. This formability analysis is usually followed by the other performance analyses during early phases of design and development. Plane strain analysis approach was chosen to simulate the formability process, for its simplicity and data availability at early phases of the vehicle development process. The developed process was used on three different automotive body side panel sections at the Rocker, A-pillar and B-pillar. The analytical results were correlated with actual measured results from a production side panel to examine the ability of the developed process in providing early design directions.

All three sections showed good correlations between measurements and analysis for the draw-in amounts. It is also clear that for draw-in amounts simulation the two draw beads modeling conditions yield close results. Even though there were some differences between the analytical strain distributions and the measurements the analytical models with draw beads provided reasonable results for design directions in terms of formability criteria. To capture the proper strain distribution or for modeling deep and complicated sections, it is necessary to model the draw bead geometry. For fast evaluation of uncomplicated shallow sections, models without draw beads can used to provide early design directions.

ACKNOWLEDGEMENT–The authors would like to thank VSAS group at General Motors Corporation for their support during the course of this work.

REFERENCES

American Iron and Steel Institute (1984). *Sheet Metal Formability.* American Iron and Steel Institute. USA.

Autoform (1999). *Autoform User's Manual*, Autoform Engineering , USA.

Cao, J. and Boyce, M. C. (1993). Draw bead penetration as a control element of material flow. *SAE Paper No.* 930517.

Hosford, W. F. and Caddell, R. M. (1993). *Metal Forming – Mechanics and Metallurgy.* Prentice Hall. NY. USA.

Keum, Y. T. and Wang, N. M. (1990). Design of automotive inner pannel by sectional forming analysis. *J. Korean Society of Automotive Technology* **12, 6,** 48–59.

Keum, Y. T., Wang, C. T., Soran, M. J. and Wagoner, R. H. (1992). Practical die design via section analysis. *Journal of Materials Technology*, **35,** 1–36.

Kobayashi, S., Oh, S. I. and Altan, T. (1989). *Metal Forming and Finite Element Method.* Oxford University Press, UK.

Soran, M. J., Keum, Y. T. and Wagoner, R. H. (1991). Section analysis with irregular tools and arbitrary draw-in conditions for numerical simulation of steel forming. *International Journal of Mechanical Science* **33, 11,** 893–909.

Wang, J., Rvachov, M. and Huo, T. (1999). 2D finite element simulation of sheet metal forming processes. *SAE Technical Paper Series*, 1001–1004.